Chemistry & Biology
Article

Distinct Prion Strains Are Defined by Amyloid Core Structure and Chaperone Binding Site Dynamics

Kendra K. Frederick,[1,2] Galia T. Debelouchina,[3,4] Can Kayatekin,[1] Tea Dorminy,[3] Angela C. Jacavone,[3,4] Robert G. Griffin,[3,4] and Susan Lindquist[1,2,5,*]
[1]Whitehead Institute for Biomedical Research, Cambridge, MA 02142, USA
[2]Howard Hughes Medical Institute, Massachusetts Institute of Technology, Cambridge, MA 02139, USA
[3]Department of Chemistry, Massachusetts Institute of Technology, Cambridge, MA 02139, USA
[4]Francis Bitter Magnet Labaratory, Massachusetts Institute of Technology, Cambridge, MA 02139, USA
[5]Department of Biology, Massachusetts Institute of Technology, Cambridge, MA 02139, USA
*Correspondence: lindquist_admin@wi.mit.edu
http://dx.doi.org/10.1016/j.chembiol.2013.12.013

SUMMARY

Yeast prions are self-templating protein-based mechanisms of inheritance whose conformational changes lead to the acquisition of diverse new phenotypes. The best studied of these is the prion domain (NM) of Sup35, which forms an amyloid that can adopt several distinct conformations (strains) that produce distinct phenotypes. Using magic-angle spinning nuclear magnetic resonance spectroscopy, we provide a detailed look at the dynamic properties of these forms over a broad range of timescales. We establish that different prion strains have distinct amyloid structures, with many side chains in different chemical environments. Surprisingly, the prion strain with a larger fraction of rigid residues also has a larger fraction of highly mobile residues. Differences in mobility correlate with differences in interaction with the prion-partitioning factor Hsp104 in vivo, perhaps explaining strain-specific differences in inheritance.

INTRODUCTION

Yeast prions are protein-based epigenetic mechanisms of inheritance (Shorter and Lindquist, 2005). They permit biological information to be encoded and inherited solely through a self-propagating conformation of a protein. Moreover, prions provide a mechanism for generating heritable phenotypic diversity that may promote survival in fluctuating environments. Indeed, a recent screen of approximately 700 wild yeasts revealed that strains recovered from diverse ecological niches harbored different prion elements, many of which conferred beneficial phenotypes in specific growth conditions (Halfmann et al., 2012). Thus, heritable differences in protein conformations represent a mechanism for the inheritance of biological traits that is used widely in nature.

The best-characterized yeast prion, [*PSI*$^+$] (Cox, 1965), is an amyloid form of the translation termination factor Sup35 (Glover et al., 1997; King and Diaz-Avalos, 2004; Paushkin et al., 1997; Tanaka et al., 2004). Amyloid formation sequesters Sup35 from the ribosome, changing the rate of stop codon read-through and creating a host of new phenotypes (True et al., 2004; True and Lindquist, 2000). The protein-remodeling factor, Hsp104, plays a critical role in this process by fragmenting replicating prion templates (Romanova and Chernoff, 2009). Together, the self-templating nature of prion conformational change and the Hsp104-governed partitioning mechanism allow prions to be inherited by daughter cells with very high fidelity (Shorter and Lindquist, 2004, 2006). Many other yeast prions are now known to share these basic mechanisms for protein-based inheritance.

Different regions of the Sup35 protein are responsible for prion templating, prion inheritance, and translation termination (Figure 1A). The N-terminal domain "N" is Q/N-rich and is required for the formation and templating of amyloid. The highly charged K/E-rich middle domain "M" promotes solubility in the nonprion form. It also contains Hsp104 binding sites (Helsen and Glover, 2012) and is required for propagon formation (Liu et al., 2002). The C-terminal domain is necessary and sufficient for translation termination. However, prion domains are modular. Transferring the NM domain to another protein creates a novel prion with phenotypes based on the NM amyloid-based sequestration of the new C terminus (Li and Lindquist, 2000). Although some studies suggest that the C-terminal domain can itself influence the prion (Krzewska et al., 2007), the NM domain contains all of the necessary features to act as a prion.

The ability of prions to propagate is afforded by the inherent and extremely efficient self-templating capacity of the amyloid, a highly ordered β sheet-rich protein polymer. The amyloid-based prion state nucleates in cells at a low frequency de novo, but once formed, efficiently propagates this change to soluble conformers (Glover et al., 1997; Patino et al., 1996). Purified NM remains soluble in solution for a long time before spontaneously forming self-seeding amyloid fibers in vitro. This lag phase can be eliminated by the addition of a small amount of preformed fibers to template the polymerization reaction (Glover et al., 1997). Remarkably, introduction of the resulting fibers alone can transform yeast to the corresponding prion state (King and Diaz-Avalos, 2004; Sparrer et al., 2000; Tanaka et al., 2004).

Interestingly, yeast prions share many features with the mammalian prion protein, PrP, the infectious agent involved in a group of deadly neurodegenerative diseases known as transmissible spongiform encephalopathies (Prusiner et al., 1998). PrP can cause pathologically distinct transmissible prion

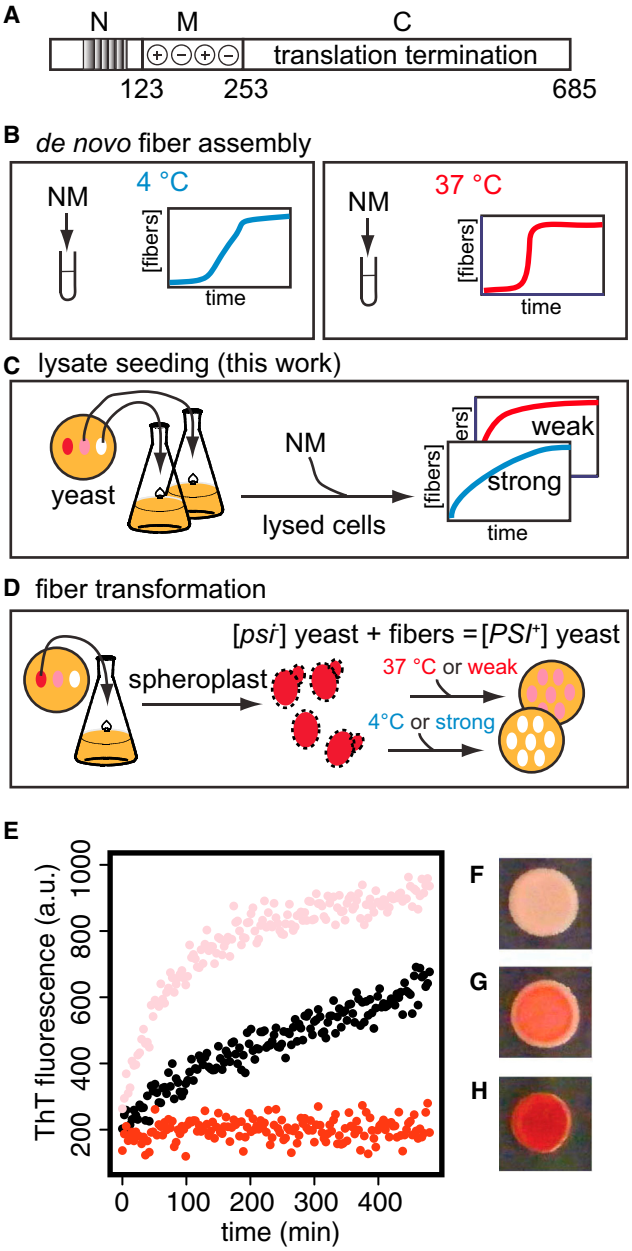

Figure 1. Regions of the Sup35 Protein

(A) Schematic diagram of the domains of the Sup35 protein.

(B) After a lag phase, purified NM spontaneously forms fibers in vitro.

(C) Fiber formation can be templated from yeast cell lysates. The character of the fibers formed matches the character of the fibers in the yeast lysate used.

(D) Introduction of NM fibers into spheroplasted [*psi*$^-$] yeast confers the [*PSI*$^+$] state in a strain-specific manner. Control of lysate-templated prion fibers.

(E) Fiber formation as monitored by Thioflavin T fluorescence for lysate-seeded NM maintains distinct kinetic character for strong (black) and weak (pink) [*PSI*$^+$] strains. Lysates from [*psi*$^-$] cells (red) do not template NM amyloid assembly.

(F–H) Introduction of lysate-templated strong fibers (F), weak fibers (G), and unpolymerized NM (H) into [*psi*$^-$] yeast cells confers expected [*PSI*$^+$] phenotypes. All 13 [*PSI*$^+$] colonies resulting from transformation with strong prion fibers had strong phenotypes and all three [*PSI*$^+$] colonies resulting from transformation with weak prion fibers had weak phenotypes.

diseases when expressed in inbred mouse lines even though the PrP proteins expressed are identical in amino acid sequence. This is because PrP can exist in a number of related, but structurally distinct prion conformations that are faithfully self-templated and produce different phenotypes. These conformational variants are called prion "strains" (Chien et al., 2004; Prusiner et al., 1998). Yeast prions can also form different strains, which have different underlying structures and distinct phenotypic consequences. That is, the prion strains act, with respect to protein-based inheritance, in a manner analogous to the genetically distinct alleles of other genes that are encoded by variations in DNA sequence. A detailed structural understanding of prion protein-based "genetic alleles" is currently lacking.

The existence of distinct prion strains was first recognized through genetic analyses. The variant phenotypes they produced were named for the strength of their read-through phenotypes and the stability of their mitotic inheritance (Derkatch et al., 1996). For example, [*psi*$^-$] strains have no suppression of the nonsense allele *ade1-14* and, due to the buildup of an adenine pathway intermediate, are red. Strong [*PSI*$^+$] strains have higher efficiency *ade1-14* suppression and are white; weak [*PSI*$^+$] strains have lower efficiency suppression and are pink. Incubation of purified NM at different temperatures (Figure 1B) biases de novo formation of fibers toward forms with different biophysical properties; fibers formed at 4°C are thermodynamically less stable than those formed at 37°C (Krishnan and Lindquist, 2005). Interestingly, introduction of the thermodynamically stronger 37°C fibers results in phenotypically weak [*PSI*$^+$] yeasts, while introduction of the biophysically weaker 4°C fibers results in phenotypically strong [*PSI*$^+$] yeasts. While this might seem counterintuitive, it has a foundation in the mechanical properties of the fibers. The physically less stable fibers are more efficiently broken by the chaperone machinery. This exposes more fiber ends for templating soluble Sup35 to the prion state, causing greater sequestration of the protein and a stronger phenotype. Moreover, because there are more propagating particles, referred to as propagons (Cox et al., 2003), the stronger [*PSI*$^+$] phenotypes are also more stable.

A variety of approaches has been used to investigate Sup35 prion structures, but a consensus structural picture has yet to emerge and we have only a minimal understanding of the differences in fiber structure associated with strong and weak prion strains. At least some part of the N domain is involved in an amyloid fold, although the arrangement of the strands within the amyloid core is still unclear. The disposition of the M domain, which is required for prion inheritance in vivo, is highly contentious, with some reports suggesting that it is mostly solvent accessible and flexible (Krishnan and Lindquist, 2005; Toyama et al., 2007) and others placing it largely within the rigid amyloid core (Shewmaker et al., 2006, 2009). These studies all used de novo-formed NM fibers (Figure 1B) that are competent to confer the [*PSI*$^+$] phenotypes to [*psi*$^-$] yeasts via fiber transformation (Figure 1D). However, de novo formed fibers contain a mix of strains and include off-pathway and noninfectious forms as well (Hess et al., 2007). Moreover, some studies used proteins with long N-terminal tags adjacent to the prion-forming domain that can influence fiber assembly (Serio et al., 2000).

In this work, we use untagged protein, eliminate conformational heterogeneity, and faithfully maintain features required

for biological prion templating and inheritance. Rather than letting the fibers assemble spontaneously, we use lysates of prion-containing cells, with well-characterized and distinct prion phenotypes (Tanaka et al., 2004), to template assembly (Figure 1C). We use magic-angle spinning (MAS) nuclear magnetic resonance (NMR) to investigate structural features of distinct prion forms in the solid state. This technique is uniquely suited to the study of protein polymers and provides quantitative structural and dynamic insights at the atomic level (Comellas and Rienstra, 2013; Debelouchina et al., 2010; Heise et al., 2005; Wasmer et al., 2009). We report characterization of both the rigid and highly dynamic portions of NM in two prion fiber forms and use fluorescence recovery after photobleaching (FRAP) to investigate the dynamics of their interaction with the Hsp104 chaperone in vivo.

RESULTS

Lysate Seeding of NM

To enrich for biologically active prion conformers, we templated NM prion fiber formation with yeast lysates of cells containing phenotypically strong [*PSI*$^{+}$] or phenotypically weak [*PSI*$^{+}$] strains (Figure 1C). To increase the starting amount of prion template in these cells, they were transformed with a high copy number plasmid encoding NM under the control of the galactose promoter and expression was induced for 6 hr before lysis. Lysates were diluted into buffer containing purified recombinant NM and incubated at 4°C (strong [*PSI*$^{+}$] lysates) or 25°C (weak [*PSI*$^{+}$] lysates and [*psi*$^{-}$] lysates) for 24 hr. These temperatures intrinsically favor the polymerization of strong and weak fiber types, respectively, reducing adventitious spontaneous formation of polymers of the wrong fiber type. To dilute away cellular constituents, reactions were sonicated and used for three sequential rounds of templated NM fiber assembly with recombinant protein. Assembly reactions were monitored by Thioflavin T fluorescence to determine the quantity of amyloid formed. The strong and weak prion fibers retained their distinct kinetic assembly properties throughout. Importantly, [*psi*$^{-}$] lysates did not seed fiber formation (Figure 1E available online).

To ensure that the fibers retained the biological properties of the initial template, we used them for "protein-only" transformation of [*psi*$^{-}$] yeast cells (Tanaka and Weissman, 2006). Introducing fibers templated by strong or weak prion forms into [*psi*$^{-}$] yeast cells conferred the expected phenotypes. Lysate-templated prion fibers faithfully transmitted strain-specific conformational information (Figure 1). To distinguish lysate-templated fibers from spontaneously polymerized preparations, we will refer to the fibers by the phenotype rather than their biophysical properties.

NM Fibers of Both Fiber Types Have Rigid and Dynamic Regions

To assess the general structural and dynamic properties of NM, we used MAS NMR spectroscopy using several different ^{13}C polarization schemes: direct polarization (DP), cross-polarization (CP), and insensitive nuclei enhanced by polarization transfer (INEPT). Lysate-templated NM fibers were assembled from purified NM proteins uniformly labeled with ^{13}C and ^{15}N. Fibers were collected by centrifugation and the glassy pellet was transferred into the NMR rotor. To normalize for small variations in the quantity of protein used in later experiments, we used one-dimensional (1D) direct polarization to report on all the ^{13}C atoms in the sample independent of the timescale of motion (Figure S1A). As expected, the spectra from strong and weak prion fibril were indistinguishable in amino acid composition and spectral resolution.

To report on rigid sites, those experiencing motion on a microsecond or longer timescale, we used the 1D ^{13}C CP scheme (Hartmann and Hahn, 1962; Hediger et al., 1994; Pines et al., 1973). Both fibril types had rigid regions with comparable apparent resolution (Figure S1B) and with peaks that were inhomogenously broadened. This is consistent with a rigid region with a complex structure, where many amino acids are in diverse rigid structural environments. The integrated intensities for the two fiber types indicated that there were fewer rigid sites in the strong prion fibers than in the weak prion fibers ($p < 10^{-7}$, student's t test). The difference in intensity was robust to small changes in experimental protocol with the weak prion fibers having about one-third more signal than the strong prion fibers ($n = 6$) over the entire experimental time course. This is in agreement with previous data using several different techniques, which have established that the amyloid core of the weak fibers is larger than that of the strong fibers (Krishnan and Lindquist, 2005; Toyama et al., 2007).

To identify and characterize the flexible, highly dynamic regions of the NM fibers (those experiencing motion on a nanosecond or shorter time scale) we used ^{13}C-detected experiments using the solution-based INEPT transfer (Burum and Ernst, 1980; Morris and Freeman, 1979). For NM fibers of both fiber types, 1D INEPT experiments resulted in spectra with intense signals, suggesting that a significant proportion of the sample experienced unconstrained motions. These strong signals were not simply a result of unpolymerized protein in the NMR samples because the lines in the INEPT spectra did not have signals for all of the amino acid types present in the protein (Heise et al., 2005). Clearly, the rigid and dynamic portions of NM contain distinct amino acids (Figure 2).

Unexpectedly, the INEPT spectrum of the strong prion fibers had a lower intensity than that of the weak prion fibers. This suggested that although proteins in the strong prion fibers had a smaller amyloid core, they also had fewer highly dynamic residues than proteins in the weak prion fibers (Figure S1C). That is, a larger portion of NM in the strong prion fibers experiences motion on an intermediate time scale that is undetectable in these experiments.

The M Domain of NM Is Highly Dynamic in Both Prion Fibril Forms

To determine whether the M domain of NM is involved in the core amyloid structure, we compared the peaks in the CP spectra (rigid residues) and INEPT spectra (dynamic residues) to NMR database values for amino acid types that are unique to the N domain or the M domain (Figure 3C; Table 1). Only the M domain contains lysines, glutamates, threonines, valines, and isoleucines (K, E, T, V, and I; Figure 2C). Together, these residues constitute more than half of the amino acids in this domain. For the strong and weak prion fibers, the 1D INEPT spectra were dominated by intense, narrow peaks with values consistent with the side chain carbons of K, E, T, V, and I (Figure 2A). The

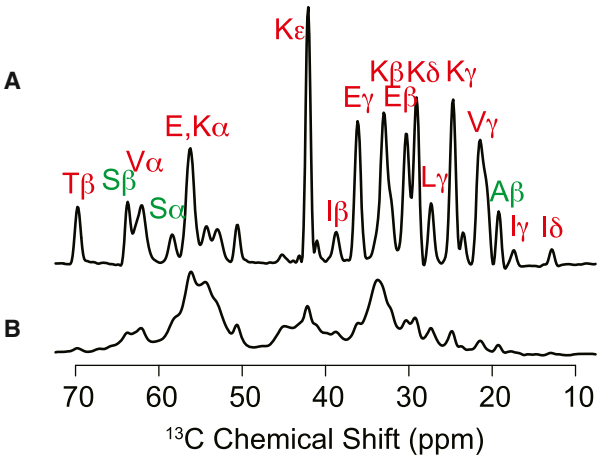

C

MSDSNQGNNQ QNYQQYSQNG NQQQGNNRYQ GYQAYNAQAQ
PAGGYYQNYQ GYSGYQQGGY QQYNPDAGYQ QQYNPQGGYQ
QYNPQGGYQQ QFNPQGGRGN YKNFNYNNNL QGYQAGFQPQ
SQGMSLNDFQ KQQKQAAPKP KKTLKLVSSS GIKLANATKK
VGTKPAESDK KEEEKSAETK EPTKEPTKVE EPVKKEEKPV
QTEEKTEEKS ELPKVEDLKI SESTHNTNNA NVTSADALIK
EQEEEVDDEV VND

Figure 2. The Dynamic Region of NM Is Localized to the M Domain

(A) The aliphatic region of the 1D INEPT spectrum of NM in the weak fiber form has multiple strong peaks with chemical shifts characteristic of the indicated amino acid atom types.

(B) These peaks are largely absent from the CP spectrum of the weak fiber form.

(C) The primary sequence of NM. Colored amino acids are those visible in the INEPT spectra, with red amino acids present only in the M domain.

See also Figure S1.

resonances in the CP spectra (Figure 2B) were devoid of residues found in the M domain. Therefore, in NM fibers of both prion fiber forms, the M domain is highly dynamic and does not participate in the amyloid core.

More of the M Domain Is Dynamic in Weak Than in Strong Prion Fibers

Having established that the M domain is overall flexible, we asked whether the flexibility of the M domain differs between the strong and weak prion fiber types. To do so, we used a ^{13}C-^{13}C INEPT-TOBSY (total through-bond correlation spectroscopy; Andronesi et al., 2005) two-dimensional (2D) correlation experiment. We combined the dynamic filter of INEPT with the transfer of polarization through the side chains with TOBSY, which allowed us to assign peaks in the spectra to spin systems of individual residue types. We assigned complete spin systems to all of the amino acid types found in the M domain of NM (Figure 3). All resonances for this region were completely consistent with random-coil chemical shift values (Wang and Jardetzky, 2002). Moreover, there are 20 tyrosine residues and 2 arginines distributed through the N domain. None of these residues gave a signal in the INEPT-TOBSY spectra, establishing that most of the N domain is not highly dynamic in either prion fibril type.

To examine the distribution of dynamic residues across the M domain, we compared integrated peak intensities for individual amino acids in the strong and weak prion fibers (Table 1). The integrated peak intensities for D, G, H, I, and Q were similar in both spectra (Figures 3F and 3G). On the other hand, integrations for A and S differed by 2-fold or more (Figure 3D); E, N, P, and T differed by more than 50% (Figure 3E); and K, L, and V differed by approximately 30% (Table 1).

To directly compare the number of mobile amino acids in the two different fiber forms, we integrated the peaks in the CC-TOBSY spectra. Cross-peaks were fit to Gaussian line shapes. Peaks for all directly connected atoms were integrated, intensities were added for each amino acid, and the sum was divided by the number of carbon atoms in each residue. To calibrate these peak intensities, we took advantage of the fact that NM contains only three isoleucines, all of which are located in the M domain. If the intensity we obtained for isoleucine corresponded to one dynamic residue, it would result in a prediction for the total number of dynamic residues that is too large for the signals in the 1D INEPT experiments. If the intensity for isoleucine corresponded to three dynamic residues, it would predict more dynamic lysines, glutamic acids, valines, and threonines than the number of these residues present in the NM sequence. Assuming that the isoleucine signal corresponds to two dynamic residues predicts reasonable values for both the signal intensity of the 1D INEPT spectra and the estimated number of dynamic amino acids in NM.

Using this calibration, the M domain for weak prion fiber has 40% more highly dynamic sites than the M domain in the strong fiber type. Thus, although much of the M domain in both fiber types is highly dynamic, there are, surprisingly, regions within this domain that are not highly mobile. Moreover, these differ between the two prion types. Specifically, the M domain of the strong prion fibers has considerably fewer highly dynamic residues than the M domain of the weak prion fibers. Because the strong prion fibers have a smaller rigid core, one might have expected that this would lead to a less constrained M domain, but this is not the case.

The N Domain in Both Fiber Types Is Rigid

To directly characterize the rigid amyloid core of NM in the strong and weak prion fiber types, we collected one-bond (20 ms mixing time) ^{13}C-^{13}C correlation spectra using proton-driven spin diffusion (PDSD; Szeverenyi et al., 1982) and one-bond (1.6 ms mixing) ^{15}N-^{13}C 2D correlation spectra using Z-filtered transferred echo double resonance (ZF-TEDOR; Hing et al., 1992; Jaroniec et al., 2002; Figure 4). The majority of the signals in both the PDSD and ZF-TEDOR experiments were consistent with amino acids in the N domain. Nearly 75% of the N domain is comprised of four amino acids: Q, N, G, and Y (Figure 2C, Table 1). Regions of the spectra for these amino acids had strong signals (Figures 4A–4D, boxes). Signals for all of the amino acids that are unique to the M domain, with the exception of one peak for a single K side chain, were absent. These results confirm that it is the N domain, and only the N domain, that is involved in the rigid amyloid core of both fiber forms.

The Rigid Regions Have Different, Well-Ordered Structures that Are a Mix of β Sheets and Turns

Many amyloid fibers are polymorphic at the molecular level, producing multiple peaks in NMR spectra for a single resonance

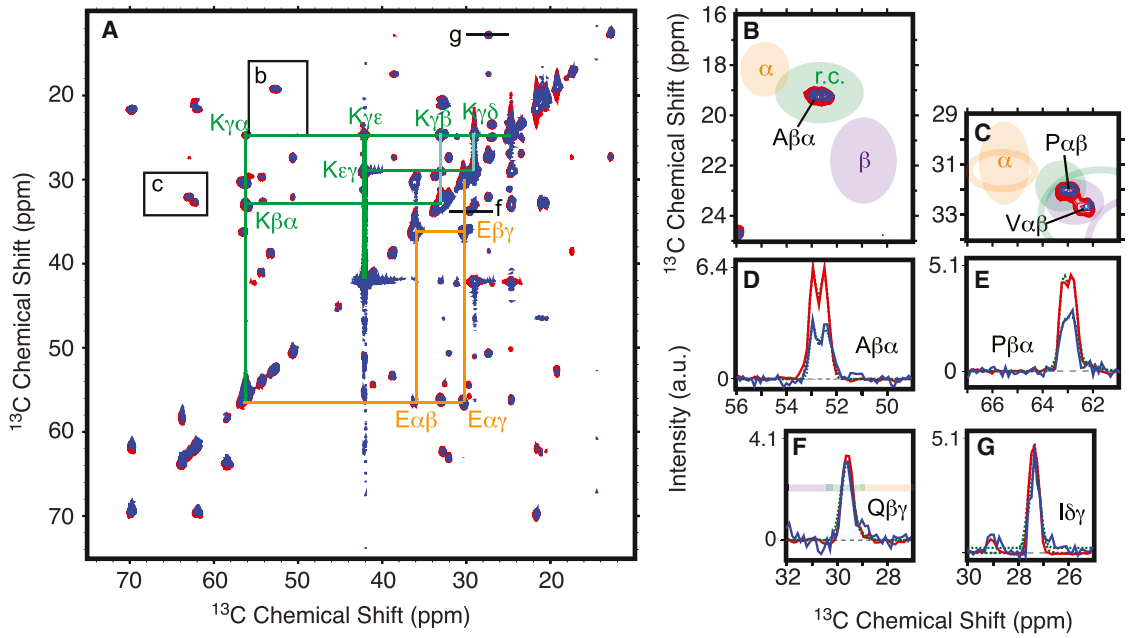

Figure 3. Weak Prion Fibers Have More Dynamic Residues Than Strong Prion Fibrils

(A) Two-dimensional ^{13}C-^{13}C INEPT-TOBSY for the strong (blue) and weak (red) prion fiber forms of uniformly ^{13}C, ^{15}N-labeled NM. Spin systems for lysine and glutamic acid are connected in green and orange, respectively.

(B and C) Expansions from (A). Ellipses indicate the average chemical shift for alpha helical (orange), random coil (green), and β sheet (purple) secondary structures. While the positions of the peaks in (A) are identical, the intensities of the peaks vary.

(D and E) One-dimensional slices through the cross peaks in (B) and (C) fit to two Gaussians (dotted line). These cross-peaks show 60 Hz of line splitting from C′-Cα J-coupling.

(F and G) However, intensities for some sites are identical. One-dimensional slices at positions indicated in (A) with Gaussian fits (dotted lines). Results of the quantification for both fiber types are reported in Table 1.

See also Figure S2 and Table S1.

(Hu et al., 2011; Paravastu et al., 2008). This did not appear to be the case for our lysate-seeded samples. While regions for abundant amino acids were crowded, regions for less numerous amino acid types had spectra that were typical for well-ordered, uniformly ^{13}C-labeled proteins, with ^{13}C line widths of ~1 ppm and ^{15}N line widths of ~2.5 ppm. Narrow lines indicate high microscopic order. Moreover, the number of peaks in well-resolved regions was equal or smaller than the number of those amino acid types in the sequence. These regions also reveal that the conformations of the amino acids in the amyloid cores differ between the weak and strong prion fibers, because the peaks were in different positions. Few peaks for the weak prion fibers (red) overlapped with those for the strong prion fiber (blue; Figures 4C and 4D). For example, the highest intensity alanines sites differed in ^{13}C chemical shift by >2 ppm, with no evidence of spectral overlap. The nonoverlapping signals indicate that these sites experience different chemical environments, providing the direct observation that the structure of NM polypeptide chains in these two different fiber forms are different.

The chemical shift is an excellent indicator of secondary structure. We compared the signals in our spectra to database values for different secondary structural elements (Wang and Jardetzky, 2002). In resolved regions, the peaks for spectra of both fiber types fell clearly in the random coil and β sheet regions, illustrating that alanine and proline residues have a mix of turn and beta secondary structure (Figure 4). Interestingly, glycines had chemical shifts consistent with, and indeed in some cases even outside of, the statistical averages for all three secondary structural elements. This suggests that glycines experience some unusual environments in the amyloid forms of NM, possibly due to tight turns that rely on the unusual conformational flexibility of glycine (due to the absence of a side chain). Due to the degenerate nature of the primary sequence of NM, we did not have site resolution for all amino acid types. We were, however, able to examine the general features of crowded regions in the spectra (Figure 4, boxes). Even in these crowded regions, the signals were predominantly consistent with random coil (turn) and β sheet secondary structure.

Weak Prion Fibers Have More Rigid Sites Than Strong Prion Fibers

Using a combination of site resolution and peak intensity, we estimated the number of each amino acid type participating in a rigid structure in the different prion fiber forms. The spectra of strong prion fibers had fewer signals than the spectra of weak prion fibers. However, most resolved peaks had similar intensities when the two spectra were compared, suggesting that the differences in the number of signals reflect changes in the number of rigid sites in the protein. For PDSD spectra, we assumed that symmetric resolved peaks with signal intensities two orders of magnitude or higher above background noise represented a single rigid site (Figures 4E and 4F;

Table 1. Amino Acid Composition and Population of Dynamic Classes

	Q	N	G	Y	R	F	P	A	S	M	D	L	H	I	V	T	E	K	All
Composition																			
N domain	35	20	21	20	2	3	7	5	4	1	2	1	0	0	0	0	0	0	121
M domain	6	7	2	0	0	1	7	9	11	1	7	7	1	3	10	11	24	25	132
Rigid																			
Strong	9	4	6	5	0	[a]	1	4	3	0	2	0	0	0	0	0	0	1	35
Weak	29	14	16	14	1	[a]	3	6	4	0	2	0	0	0	0	0	2	1	92
Intermediate																			
Strong	30	20	15	15	2	[a]	9	8	8	2	4	6	0	1	5	6	12	6	153
Weak	10	9	5	6	1	[a]	5	7	3	2	5	5	0	1	3	3	5	1	70
Dynamic																			
Strong	2	3	2	0	0	0	4	2	4	0	3	2	1	2	5	5	12	18	65
Weak	2	4	2	0	0	0	6	5	8	0	2	3	1	2	7	8	17	23	91

[a]Phenylalanine is degenerate with tyrosine.

Figure S2; Table 1). For ZF-TEDOR, resolved sites with a signal intensity and order of magnitude above the background noise of the spectra were assumed to represent a single site. The cross-peaks used for quantization of each side chain are given in Table S1.

Peak intensities for Q and N were higher by almost an order of magnitude than those for less abundant residues in PDSD spectra. For G, intensities were larger than other residues by a factor of 3 to 5. Such intensity differences can arise for a variety of reasons, including differences in dynamic motions, static conformational disorder. However, given the large number of these three amino acid types in this protein, the increased intensity is likely a result of several amino acids having very similar chemical shifts. For Q, N, and G, the signal in the boxed areas (Figures 4A and 4B) was integrated and the number of rigid residues was conservatively estimated by assuming that the values of the most intense resolved sites represented a maximum signal in these experiments for a single site. The results of this integration approximate the lower limit of the number of rigid sites in each fiber type. Counting peaks in this way indicated that the number of residues in a rigid structure in the weak prion fibers was nearly twice as large as in the strong prion fiber.

Localization of Rigid, Intermediate, and Dynamic Regions

While we have reasonable estimates for the number of amino acids that are rigid, dynamic, or moving on an intermediate timescale, we do not have sequence-specific information. However, relying on the fact that adjacent amino acids often have similar dynamic properties, together with NM's unusual amino acid sequence, we set out to computationally determine which sections of the molecule were most likely to participate in each dynamic class. The proline, alanine, and serine residues were key to this analysis. These residues participated in all three dynamic classes (Table 1). They are also relatively rare in the NM sequence, and yet are spread throughout the protein (Figure 2C). Similar computational approaches were previously used to determine which regions of a different yeast prion fibril, Ure2p1, were likely involved in the amyloid core (Baxa et al., 2007).

To reduce the computational burden of a brute force approach, we applied a heuristic model that treated the primary sequence as blocks of six amino acids. Every residue in each block was assigned to the same dynamic class. We defined a function, Δ, as the absolute values of the difference between the experimentally determined number of amino acids in each class, $E_{aa,class}$ (Table 1) and the number of amino acids in each class for each proposed arrangement $C_{aa,class}$:

$$\Delta \equiv \sum_{aa} \sum_{class} \left| \left(E_{aa,class} - C_{aa,class} \right) \right|. \qquad \text{(Equation 1)}$$

The proposed arrangements were scored by looking for the closest match of amino acids in each class to the experimentally determined values in Table 1. Data were preprocessed to eliminate testing possibilities above a threshold energy, which is largely driven by violations of the number of residues in a particular class. Preprocessing eliminated the testing of ~30% of the possible iterations. To avoid bias from the artificially imposed block boundaries, the calculation was repeated with six amino acid-long blocks starting at residues 3 or 5 instead of residue 1. We generated a collection of likely dynamic arrangements for blocks of length 2 from all combinations of the dynamic class assignments that occurred at least once in the collection of lowest Δ arrangements. The Δ was calculated for the selected block 2 arrangements and the fraction of lowest Δ arrangements for each dynamic class is reported in Figure 5.

The resulting models, arrived at in an unbiased fashion, gave the most likely placement of rigid, intermediate, and dynamic regions (Figure 5). The N domain had a mix of rigid and intermediate sites. Within the N domain, the N-terminal-most residues were likely to be rigid in both prion forms. The largest differences between fiber types in the N domain were found in the oligopeptide repeat and adjacent regions. In these regions, the weak prion fiber was largely predicted to be rigid and the strong prion fiber was predicted to be experiencing motion on an intermediate timescale. The M domain had a mix of dynamic and intermediate sites. The C-terminal portion of the M domain was predicted to be moving on the intermediate timescale in both fiber types. Intriguingly, the largest difference between fiber forms in the M domain, where the weak prion fiber form was likely

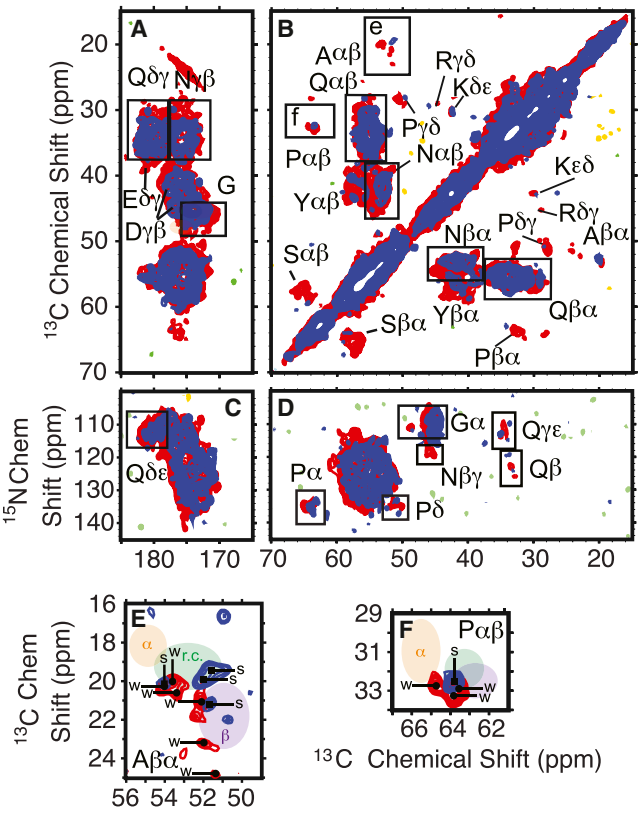

Figure 4. Weak Prion Fibers Have More Rigid Sites Than Strong Prion Fibers

The rigid portions of both fiber forms have β sheet or random coil secondary structure.

(A) 2D PDSD ^{13}C-^{13}C correlation spectra of the weak (red) and strong (blue) prion fibers of uniformly ^{13}C- and ^{15}N-labeled NM with a 20 ms mixing time (one bond) for the carbonyl carbon region. Spectra are all shown at comparable contour levels, clearly demonstrating the increased intensity in the weak fiber spectra.

(B) The aliphatic region of the PDSD spectra in (A). Strong cross-peaks are indicated with amino acid type assignments.

(C) Carbonyl region of a heteronuclear ^{15}N-^{13}C correlation experiment (TEDOR) with a 1.6 ms (one bond) mixing time.

(D) Aliphatic region of the spectra in (C).

(E and F) Expansions of the indicated areas in (B). Colored ellipses indicate expected chemical shifts for alpha helical (orange), random coil (green), and β sheet (purple) secondary structure.

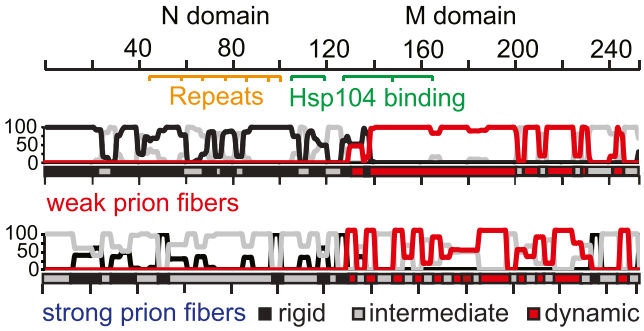

Figure 5. Computational Fitting Localizes Rigid, Intermediate, and Dynamic Regions

Fraction of lowest energy arrangement with indicated dynamic class assignment is indicated for each position in NM. Assignments that are most likely dynamic are represented by colored bars.

to be dynamic and the strong prion fiber form to be in intermediate exchange (Figure 5), was at a region previously identified as an Hsp104 binding site (Helsen and Glover, 2012).

In Vivo, More Hsp104 Is Bound to Weak Prion Fibers Than Strong Prion Fibers

To determine whether there might be dynamic differences in the interaction of Hsp104 with weak and strong prions in vivo, we used fluorescence recovery after photobleaching (FRAP). We analyzed cells carrying strong and weak [*PSI*$^+$] prions and expressing an Hsp104-mCherry fusion under the control of the endogenous promoter of Hsp104. The fusion protein had the same capacity to faithfully propagate the Sup35 prion as wild-type Hsp104 (Figure S3).

The cells also carried a centromeric plasmid encoding NM-GFP under the control of the galactose promoter. To depict NM-GFP after capture by pre-existing [*PSI*$^+$] elements, NM-GFP expression was induced for a few hours by transferring the cells to galactose media. As expected, Hsp104-mCherry colocalized with the NM-GFP foci. The Hsp104-mCherry fluorescence in these foci was bleached to 50%–20% of its original intensity. The recovery of mCherry fluorescence was measured as a function of time. Image acquisition produced little or no additional photobleaching.

For foci templated by both the strong and weak prion types, the rate of FRAP for Hsp104-mCherry, as measured by the $t_{1/2}$, was similar. That is, the kinetics of exchange between [*PSI*$^+$]-bound Hsp104 and the soluble pool of Hsp104 was similar for the different fiber types in vivo. Conversely, the immobile fraction of Hsp104—the proportion of molecules that did not exchange with the free pool of unbound Hsp104—was significantly greater for the weak prion types (46 ± 1%) compared to the strong prion types (34 ± 2%; Figure 6). Thus, there must be at least two classes of binding sites for Hsp104 on prion assemblies. One of these is similar for the two prion types and is readily exchangeable with the free pool of Hsp104. The other is more tightly bound and weak prions contain a greater fraction of such sites.

DISCUSSION

Yeast prions represent a paradigm-shifting, protein-based mechanism for the inheritance of biological phenotypes. The strong and weak prion strains of Sup35 confer distinct heritable phenotypes analogous to the distinct phenotypes conferred by allelic differences in DNA sequence. They are, however, based on different self-templating amyloid conformations of the same protein. The inheritance of both prion types is governed by intimate relations with the cellular chaperone machinery, with Hsp104 playing a particularly important role. Despite intense study, we still have only a rudimentary understanding of the structural differences that underpin the inheritance of distinct phenotypes. Using MAS NMR spectroscopy, we establish that the region of the prion that drives heritable, strain-specific differences in prion polymerization (the N-terminal amyloid domain) has a distinct structure in different strains. Many side chains

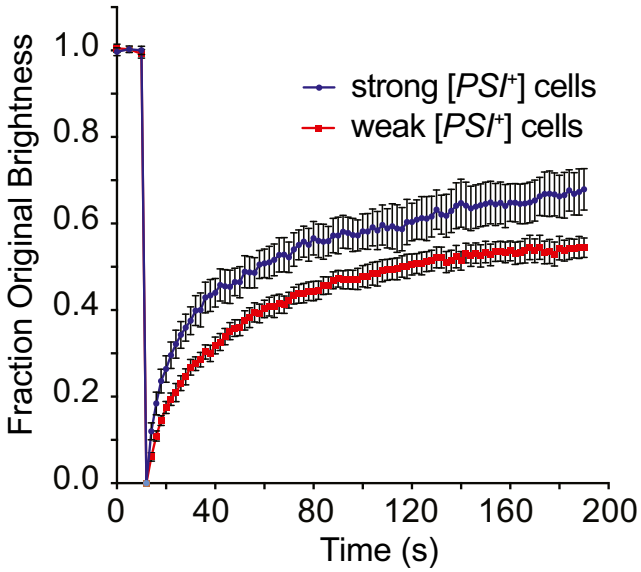

Figure 6. More Hsp104 Binds to Weak Prion Fibers Than to Strong Prion Fibers In Vivo

The fluorescence recovery after photobleaching curves for Hsp104-mCherry containing foci in strong (blue) and weak (red) [*PSI*$^+$] are shown. The traces were normalized for both the initial intensity and the depth of photobleaching. Figure S3 shows that Hsp104-mCherry does not affect chaperone function. Error bars represent SEM.

exhibit distinct chemical shifts, indicating that they are in different chemical environments. We also find that the regions that do not participate in the amyloid are also structurally distinct, with very different dynamic properties, particularly in a segment previously identified as a key interaction site for Hsp104. Indeed, using fluorescence recovery after photobleaching, we establish differences in the nature of interaction of Hsp104 with the two prion types in vivo.

Previous work had established that the N-terminal domain forms the amyloid core of de novo NM fibers and that the core of fibers formed at 4°C is shorter than that of fibers formed at higher temperatures (Krishnan and Lindquist, 2005; Toyama et al., 2007). Fibers formed at 4°C are biased toward structures that confer strong prion phenotypes in vivo, while fibers formed at higher temperatures are biased toward structures that confer weaker phenotypes. Although spontaneously assembling fibers always contain some mixture of forms, work with such material made substantial contributions to our understanding of strain-specific differences in inheritance. In contrast to previous work, we used fibers templated from prions formed in vivo, with well-characterized and highly reproducible biological phenotypes. Also in contrast with previous studies, which used indirect labeling or deuterium-exchange techniques, we used NMR to directly observe the amino acid side chains of such fibers. This revealed that the amyloid core of the strong prion fiber is somewhat smaller and that of the weak prion fiber is considerably larger than those defined previously. More importantly, our data directly establish that the larger amyloid core of the weak prion fibers is structurally distinct from that of the strong prion fibers, and not simply an extension of a shared common structure.

For both prion forms, we observed resolved peaks with different chemical shifts, reflecting different well-ordered environments. Striking differences in the intercalations of the side chains have been described in microcrystals formed from small pieces of the N domain, suggesting they might be the basis of strain-specific differences in prion inheritance (Sawaya et al., 2007; Wiltzius et al., 2009). However, the biological correlates of these structures were never determined. Changes in the assembly kinetics of a collection of several NM mutants also suggested that the structures of the amyloid core likely differ between fiber forms (Toyama et al., 2007). Here, we establish directly that the two prion types do indeed have distinct amyloid structures, with many side chains in different chemical environments.

Unlike the N domain, considerable confusion exists about the fundamental nature of the M domain of the NM prion. It has been alternatively reported to be flexible (Krishnan and Lindquist, 2005; Toyama et al., 2007) or to be primarily in a rigid parallel-in-register amyloid core (Shewmaker et al., 2006, 2009). We do not know what accounts for these discrepancies. They might reflect the use of fibers assembled de novo, which contain heterogeneous mixtures of multiple fiber forms (Hess et al., 2007; Shewmaker et al., 2009; Toyama et al., 2007) or simply the liabilities in the interpretation of experimental outputs from the distinct techniques used. For example, the previous NMR study focused on a single amino acid type, labeled only at one backbone atom position. We have analyzed instead the dynamic properties of the side chains. Rigorously, we cannot exclude the possibly that the backbone somehow remains rigid, but we clearly establish that the amino acid side chains in the M domain of both prion fiber forms are highly dynamic. The chemical shifts establish that they are neither in an alpha helical nor a β sheet structure, but have the character of a random coil. Furthermore, more of the M domain is dynamic in the weak prion fibers than in the strong prion fibers. We also infer that a portion of the M domain experiences motion on an intermediate time scale.

Differences in the dynamic properties of the M domain likely have important biological ramifications for the two prion types. In vivo, strong and weak strains of NM have different inheritance patterns and the M domain is implicated in propagon formation, which is important for stable inheritance of the prion (Liu et al., 2002). In vitro, the M domain contains the primary Hsp104 binding sites (Helsen and Glover, 2012) and mutations in this region prevent curing by overexpression of Hsp104. Together, these results suggest that the M domain contains a key site involved in Hsp104-mediated prion severing activity, a requirement for prion inheritance. Moreover, nucleotide hydrolysis and hexamer subunit co-operativity requirements of Hsp104 are distinct for fragmentation of the two fiber forms in vitro (DeSantis et al., 2012). Specifically, the weak prion fiber types require the cooperative activity of more than six Hsp104 monomers, indicative of more than one hexamer being required to fragment these fibers. Computational fitting of our data to the Sup35 sequence points to differences in mobility of the M domain of prion fibers occurring at the previously identified Hsp104 binding site. Furthermore, our fluorescence recovery after the photobleaching experiments indicates that a larger fraction of Hsp104 molecules associated with the weak prion fibers do not undergo rapid

exchange with the free pool of Hsp104. This observation suggests conformational accessibility may drive distinct modes of interaction with Hsp104.

Strong and weak [*PSI*$^+$] strains have different stop-codon read-through phenotypes. Sup35 expression levels are the same in [*psi*$^-$] and [*PSI*$^+$] cells, as they are in weak and strong [*PSI*$^+$] strains. The differences in phenotype are caused by having differing amounts of soluble Sup35 available for translation termination (Uptain et al., 2001). Recruitment of monomers into the amyloid fiber is limited not by the rate of templating per se, but by the number of free templating ends available from fiber fragmentation. NM fibers producing strong phenotypes are thermodynamically less stable and more easily fragmented. They recruit a greater fraction of Sup35 monomers into the amyloid form and produce a stronger phenotype. Conversely, NM fibers producing weak phenotypes are more stable, recruit fewer monomers, and leave behind a larger pool of functional Sup35. Although weak prion strains have less of the protein in the amyloid state, our results indicate that weak prion fibers contain the greater amount of bound Hsp104. Therefore, the fraction of Sup35 that is in the prion form cannot be the sole determinant of Hsp104 binding. Instead, we suggest that the properties that drive Hsp104 binding to NM are also encoded in the dynamic differences of the prion fiber types. A mixture of rigid and mobile regions may prove to be a general feature of prion inheritance; mutations that increase solution-state rigidity of a fragment containing the second repeat in the N domain are associated with impaired prion propagation (Marchante et al., 2013). Thus, prion strain differences may be encoded by differences in the structure of the amyloid core as well as by differences in the dynamics of the chaperone binding sites.

Despite differences in the population of NM in each dynamic class, strong and weak prion fibers share some common features. In both forms, a single, compact, well-defined folded domain is seen alongside a second disordered segment that lacks tertiary structure and is highly dynamic. This is an organization strategy seen in another functional amyloid Het-s (Wasmer et al., 2009), as well as for proteins of disease-associated amyloids such as a-syn (Heise et al., 2005) and PrP (Helmus et al., 2010). In the case of NM, at least, the organization of the rigid and dynamic regions may be particularly important to maintain the prion strains. The prion form of Sup35 can be eliminated either by deletion or overexpression of Hsp104. Therefore, for an amyloid form of NM to be a prion, interactions with the chaperone machinery must be sufficient to create propagons but not so strong as to eliminate the amyloid form altogether. Our work suggests that chaperone interactions may be mediated by dynamic information encoded in the prion conformation.

SIGNIFICANCE

Yeast prions are self-templating, protein-based genetic elements whose conformational changes enable enhanced phenotypic diversity. One of the best-studied prions, [*PSI*$^+$], results from the sequestration of Sup35 in a heritable amyloid state, leading to the reduction of translation termination efficiency. Most prions, including [*PSI*$^+$], exhibit stable phenotypic changes of varying magnitudes called "strains." The strength of a strain is determined by the delicate interplay between the thermodynamic stability of the intermolecular interactions between protein monomers and the activity of the prion propagation machinery that fragments the fibers. Using magic angle spinning solid-state nuclear magnetic resonance spectroscopy, we provide direct, detailed structural observations of two different phenotypic strains of [*PSI*$^+$] over a broad range of timescales. Using lysate templated fibrils to replicate the in vivo structure, we confirm that the two strains differ in the size of the rigid amyloid core and, more importantly establish that the amyloid cores have different structures. Additionally, we discovered that the more thermodynamically stable fibers, which give rise to weak [*PSI*$^+$], harbor regions of more dynamic residues compared to less stable fibers that give rise to strong [*PSI*$^+$]. These dynamic regions seem to enable increased access of chaperones involved in fiber fragmentation. Thus, stable prion states are limited by both the number of potential conformations capable of forming a heritable amyloid core and also by a structure with sufficient dynamic regions to enable the binding of disaggregating chaperones.

EXPERIMENTAL PROCEDURES

Sample Preparation

Recombinant prion domain of the yeast prion protein (NM) was expressed in M9 minimal media and purified as described elsewhere (Serio et al., 1999). Uniformly ^{13}C- and ^{15}N-labeled NM samples were prepared by growing BL21(DES)-Rosetta *Esherichia coli* in the presence of minimal media enriched with 1 g/l $^{15}NH_4Cl$ and 2 g/l D-glucose $^{13}C_6$ (Cambridge Isotope Labs). A concentrated stock solution of purified NM in 6 M GdHCl was boiled for 10 min, then diluted at least 120-fold into NM assembly buffer (5 mM potassium phosphate pH 7.5, 150 mM NaCl) pre-equilibrated at either 4°C or 37°C and containing lysate-derived NM seeds (see below) at 2.5% (monomer concentration) and allowed to assemble at 4°C or 37°C for the strong and weak prion fibers respectively, quiescent for 48 hr. Fibers were pelleted by ultracentrifugation at 500,000 × *g* for 1 hr at 15°C, washed with 5 mM KPi pH 7.5, and collected by centrifugation at 430,000 × *g* for 1 hr at 15°C. Twenty milligrams of hydrated pellet were packed into a Varian 3.2 mm rotor (Revolution NMR).

Lysate Seeding

Yeast cells manifesting a [*psi*$^-$], weak [*PSI*$^+$], or strong [*PSI*$^+$] *ade1-14* read-through phenotype were transformed with a 2 μm plasmid with NM behind the galactose promotor. Cells were grown in a 50 ml culture volume to mid-log phase in SD-raffinose and NM production was induced by the addition of 2% galactose to the media for 6 hr. Cells were collected by centrifugation, washed in water, and pellets were flash-frozen. Cell pellets were resuspended in 250 μl of lysis buffer (50 mM Tris pH 7.4, 200 mM NaCl, 2 mM TCEP, 5% glycerol, 1 mM EDTA, 4 mM PMSF, 5 μg/ml aprotinin, 5 μg/ml leupeptin, and one protease inhibitor cocktail pellet [Roche]) with an equal volume of acid-washed glass beads. Cells were lysed by bead beading for 8 min at 4°C. Lysates were diluted 1:5 into 5 mM potassium phosphate pH 7.5 and 150 mM NaCl. Purified NM was diluted at least 100-fold out of 6 M GdHCl to a final concentration of 5 μM and reactions were incubated without shaking at 4°C (strong lysates) or 25°C (weak lysates) for 24 hr. Reactions were sonicated (power level 3, 50% duty cycle, 30 s) and used as a template for NM fiber formation at 5% of the reaction volume three times, successively diluting away cellular constituents, before being used to seed NMR samples of purified uniformly isotopically enriched protein. As a control, during preparation of seeds, assembly reactions were monitored for Thioflavin T fluorescence; [*psi*$^-$] lysates did not seed fiber formation (Figure 1E). Fiber transformations were done as described (Tanaka and Weissman, 2006) using quiescent, lysate-seeded reactions. As expected, transformation efficiencies were low (under 2%) but true to type.

MAS NMR Spectroscopy

Experiments were performed with a custom designed spectrometer (courtesy of D.J. Ruben, Francis Bitter Magnet Laboratory, Massachusetts Institute of Technology, Cambridge, MA) operating at 700 MHz ^{1}H Larmor frequency equipped with a triple resonance ^{1}H/^{13}C/^{15}N Varian Chemagnetics 3.2 mm probe (Agilent). The sample was cooled with a stream of dry air maintained at a temperature of 0°C, while we estimate that the sample temperature was 10°C to 15°C higher. The spectra were recorded at 12.5 kHz MAS. The mixing period for ^{13}C-^{13}C 2D correlation spectra was set to 20 ms. ^{15}N-^{13}C correlations were recorded with TEDOR dipolar recoupling with a mixing period of 1.6 ms. All recycle delays were set to 3 s, except for the direct polarization experiments that had a recycle day of 10 s. All spectra were processed in NMRpipe (Delaglio et al., 1995) and analyzed using Sparky (T.D. Goddard and D.G. Kneller, University of California, San Francisco).

Fluorescence Recovery after Photobleaching

A w303 yeast strain was transformed with a CEN plasmid containing C-terminally mCherry-tagged Hsp104 under the endogenous promoter. This strain was then crossed to either the strong or weak [*PSI*$^{+}$] yeast strains used for the NMR experiments. Yeast growing in log phase were mounted on a glass side with the growth medium and subjected to FRAP with an Andor Revolution spinning disk confocal microscope using a 60X oil immersion lens and the 561 nm excitation line. The single observable focus in the cell was bleached with a 750 microsecond pulse at 40% of maximum laser intensity, resulting in a 50%–80% loss of fluorescence intensity. Recovery from photobleaching was then measured every 5 s, with a 1 s exposure time. Little or no additional photobleaching was observed during imaging. All data were normalized, both for photobleaching and for bleach depth, and fit using the easyFRAP software package (Rapsomaniki et al., 2012).

SUPPLEMENTAL INFORMATION

Supplemental Information includes three figures and one table and can be found with this article online at http://dx.doi.org/10.1016/j.chembiol.2013.12.013.

AUTHOR CONTRIBUTIONS

K.K.F. initiated the project; K.K.F. and G.T.D. designed and carried out NMR experiments and data analysis; K.K.F., A.C.J., and C.K. designed and carried out biochemical experiments; K.K.F. and T.D. designed and carried out computational modeling; R.G.G. and S.L. supervised the projects and interpreted the results; and K.K.F. and S.L. wrote the paper.

ACKNOWLEDGMENTS

We thank members of the Lindquist and Griffin laboratories for comments on the manuscript. We thank Dr. Marvin Bayro for helpful discussions and Dr. Yossi Farjoun for input on algorithm design. S.L. is an investigator of the Howard Hughes Medical Institute. K.K.F. is an HHMI fellow of the Life Science Research Foundation. This work was supported by US National Institutes of Health grants GM025874 to S.L. and EB003151 and EB002026 to R.G.G.

Received: September 4, 2013
Revised: November 14, 2013
Accepted: December 12, 2013
Published: January 30, 2014

REFERENCES

Andronesi, O.C., Becker, S., Seidel, K., Heise, H., Young, H.S., and Baldus, M. (2005). Determination of membrane protein structure and dynamics by magic-angle-spinning solid-state NMR spectroscopy. J. Am. Chem. Soc. *127*, 12965–12974.

Baxa, U., Wickner, R.B., Steven, A.C., Anderson, D.E., Marekov, L.N., Yau, W.M., and Tycko, R. (2007). Characterization of beta-sheet structure in Ure2p1-89 yeast prion fibrils by solid-state nuclear magnetic resonance. Biochemistry *46*, 13149–13162.

Burum, D.P., and Ernst, R.R. (1980). Net polarization transfer via a j-ordered state for signal enhancement of low-sensitivity nuclei. J. Magn. Reson. *39*, 163–168.

Chien, P., Weissman, J.S., and DePace, A.H. (2004). Emerging principles of conformation-based prion inheritance. Annu. Rev. Biochem. *73*, 617–656.

Comellas, G., and Rienstra, C.M. (2013). Protein structure determination by magic-angle spinning solid-state NMR, and insights into the formation, structure, and stability of amyloid fibrils. Annu Rev Biophys *42*, 515–536.

Cox, B.S. (1965). PSI, A cytoplasmic suppressor of super-suppressor in yeast. Heredity *20*, 505–521.

Cox, B., Ness, F., and Tuite, M. (2003). Analysis of the generation and segregation of propagons: entities that propagate the [PSI+] prion in yeast. Genetics *165*, 23–33.

Debelouchina, G.T., Platt, G.W., Bayro, M.J., Radford, S.E., and Griffin, R.G. (2010). Magic angle spinning NMR analysis of beta2-microglobulin amyloid fibrils in two distinct morphologies. J. Am. Chem. Soc. *132*, 10414–10423.

Delaglio, F., Grzesiek, S., Vuister, G.W., Zhu, G., Pfeifer, J., and Bax, A. (1995). NMRPipe: a multidimensional spectral processing system based on UNIX pipes. J. Biomol. NMR *6*, 277–293.

Derkatch, I.L., Chernoff, Y.O., Kushnirov, V.V., Inge-Vechtomov, S.G., and Liebman, S.W. (1996). Genesis and variability of [PSI] prion factors in Saccharomyces cerevisiae. Genetics *144*, 1375–1386.

DeSantis, M.E., Leung, E.H., Sweeny, E.A., Jackrel, M.E., Cushman-Nick, M., Neuhaus-Follini, A., Vashist, S., Sochor, M.A., Knight, M.N., and Shorter, J. (2012). Operational plasticity enables hsp104 to disaggregate diverse amyloid and nonamyloid clients. Cell *151*, 778–793.

Glover, J.R., Kowal, A.S., Schirmer, E.C., Patino, M.M., Liu, J.J., and Lindquist, S. (1997). Self-seeded fibers formed by Sup35, the protein determinant of [PSI+], a heritable prion-like factor of S. cerevisiae. Cell *89*, 811–819.

Halfmann, R., Jarosz, D.F., Jones, S.K., Chang, A., Lancaster, A.K., and Lindquist, S. (2012). Prions are a common mechanism for phenotypic inheritance in wild yeasts. Nature *482*, 363–368.

Hartmann, S.R., and Hahn, E.L. (1962). Nuclear double resonance in rotating frame. Phys. Rev. *128*, 2042.

Hediger, S., Meier, B.H., Kurur, N.D., Bodenhausen, G., and Ernst, R.R. (1994). NMR cross-polarization by adiabatic passage through the Hartmann-Hahn condition (aphh). Chem. Phys. Lett. *223*, 283–288.

Heise, H., Hoyer, W., Becker, S., Andronesi, O.C., Riedel, D., and Baldus, M. (2005). Molecular-level secondary structure, polymorphism, and dynamics of full-length alpha-synuclein fibrils studied by solid-state NMR. Proc. Natl. Acad. Sci. USA *102*, 15871–15876.

Helmus, J.J., Surewicz, K., Surewicz, W.K., and Jaroniec, C.P. (2010). Conformational flexibility of Y145Stop human prion protein amyloid fibrils probed by solid-state nuclear magnetic resonance spectroscopy. J. Am. Chem. Soc. *132*, 2393–2403.

Helsen, C.W., and Glover, J.R. (2012). Insight into molecular basis of curing of [PSI+] prion by overexpression of 104-kDa heat shock protein (Hsp104). J. Biol. Chem. *287*, 542–556.

Hess, S., Lindquist, S.L., and Scheibel, T. (2007). Alternative assembly pathways of the amyloidogenic yeast prion determinant Sup35-NM. EMBO Rep. *8*, 1196–1201.

Hing, A.W., Vega, S., and Schaefer, J. (1992). Transferred-echo double-resonance NMR. J. Magn. Reson. *96*, 205–209.

Hu, K.N., McGlinchey, R.P., Wickner, R.B., and Tycko, R. (2011). Segmental polymorphism in a functional amyloid. Biophys. J. *101*, 2242–2250.

Jaroniec, C.P., Filip, C., and Griffin, R.G. (2002). 3D TEDOR NMR experiments for the simultaneous measurement of multiple carbon-nitrogen distances in uniformly (13)C,(15)N-labeled solids. J. Am. Chem. Soc. *124*, 10728–10742.

King, C.Y., and Diaz-Avalos, R. (2004). Protein-only transmission of three yeast prion strains. Nature *428*, 319–323.

Krishnan, R., and Lindquist, S.L. (2005). Structural insights into a yeast prion illuminate nucleation and strain diversity. Nature *435*, 765–772.

Krzewska, J., Tanaka, M., Burston, S.G., and Melki, R. (2007). Biochemical and functional analysis of the assembly of full-length Sup35p and its prion-forming domain. J. Biol. Chem. *282*, 1679–1686.

Li, L., and Lindquist, S. (2000). Creating a protein-based element of inheritance. Science *287*, 661–664.

Liu, J.J., Sondheimer, N., and Lindquist, S.L. (2002). Changes in the middle region of Sup35 profoundly alter the nature of epigenetic inheritance for the yeast prion [PSI+]. Proc. Natl. Acad. Sci. USA *99*, 16446–16453.

Marchante, R., Rowe, M., Zenthon, J., Howard, M.J., and Tuite, M.F. (2013). Structural definition is important for the propagation of the yeast [PSI+] prion. Mol. Cell *50*, 675–685.

Morris, G.A., and Freeman, R. (1979). Enhancement of Nuclear Magnetic-Resonance Signals by Polarization Transfer. J. Am. Chem. Soc. *101*, 760–762.

Paravastu, A.K., Leapman, R.D., Yau, W.M., and Tycko, R. (2008). Molecular structural basis for polymorphism in Alzheimer's beta-amyloid fibrils. Proc. Natl. Acad. Sci. USA *105*, 18349–18354.

Patino, M.M., Liu, J.J., Glover, J.R., and Lindquist, S. (1996). Support for the prion hypothesis for inheritance of a phenotypic trait in yeast. Science *273*, 622–626.

Paushkin, S.V., Kushnirov, V.V., Smirnov, V.N., and Ter-Avanesyan, M.D. (1997). In vitro propagation of the prion-like state of yeast Sup35 protein. Science *277*, 381–383.

Pines, A., Gibby, M.G., and Waugh, J.S. (1973). Proton-enhanced NMR of dilute spins in solids. J. Chem. Phys. *59*, 569–590.

Prusiner, S.B., Scott, M.R., DeArmond, S.J., and Cohen, F.E. (1998). Prion protein biology. Cell *93*, 337–348.

Rapsomaniki, M.A., Kotsantis, P., Symeonidou, I.E., Giakoumakis, N.N., Taraviras, S., and Lygerou, Z. (2012). easyFRAP: an interactive, easy-to-use tool for qualitative and quantitative analysis of FRAP data. Bioinformatics *28*, 1800–1801.

Romanova, N.V., and Chernoff, Y.O. (2009). Hsp104 and prion propagation. Protein Pept. Lett. *16*, 598–605.

Sawaya, M.R., Sambashivan, S., Nelson, R., Ivanova, M.I., Sievers, S.A., Apostol, M.I., Thompson, M.J., Balbirnie, M., Wiltzius, J.J.W., McFarlane, H.T., et al. (2007). Atomic structures of amyloid cross-beta spines reveal varied steric zippers. Nature *447*, 453–457.

Serio, T.R., Cashikar, A.G., Moslehi, J.J., Kowal, A.S., and Lindquist, S.L. (1999). Yeast prion [psi +] and its determinant, Sup35p. Methods Enzymol. *309*, 649–673.

Serio, T.R., Cashikar, A.G., Kowal, A.S., Sawicki, G.J., Moslehi, J.J., Serpell, L., Arnsdorf, M.F., and Lindquist, S.L. (2000). Nucleated conformational conversion and the replication of conformational information by a prion determinant. Science *289*, 1317–1321.

Shewmaker, F., Wickner, R.B., and Tycko, R. (2006). Amyloid of the prion domain of Sup35p has an in-register parallel beta-sheet structure. Proc. Natl. Acad. Sci. USA *103*, 19754–19759.

Shewmaker, F., Kryndushkin, D., Chen, B., Tycko, R., and Wickner, R.B. (2009). Two prion variants of Sup35p have in-register parallel beta-sheet structures, independent of hydration. Biochemistry *48*, 5074–5082.

Shorter, J., and Lindquist, S. (2004). Hsp104 catalyzes formation and elimination of self-replicating Sup35 prion conformers. Science *304*, 1793–1797.

Shorter, J., and Lindquist, S. (2005). Prions as adaptive conduits of memory and inheritance. Nat. Rev. Genet. *6*, 435–450.

Shorter, J., and Lindquist, S. (2006). Destruction or potentiation of different prions catalyzed by similar Hsp104 remodeling activities. Mol. Cell *23*, 425–438.

Sparrer, H.E., Santoso, A., Szoka, F.C., Jr., and Weissman, J.S. (2000). Evidence for the prion hypothesis: induction of the yeast [PSI+] factor by in vitro- converted Sup35 protein. Science *289*, 595–599.

Szeverenyi, N.M., Sullivan, M.J., and Maciel, G.E. (1982). Observation of spin exchange by two-dimensional fourier-transform C-13 cross polarization-magic-angle spinning. J. Magn. Reson. *47*, 462–475.

Tanaka, M., and Weissman, J.S. (2006). An efficient protein transformation protocol for introducing prions into yeast. Methods Enzymol. *412*, 185–200.

Tanaka, M., Chien, P., Naber, N., Cooke, R., and Weissman, J.S. (2004). Conformational variations in an infectious protein determine prion strain differences. Nature *428*, 323–328.

Toyama, B.H., Kelly, M.J., Gross, J.D., and Weissman, J.S. (2007). The structural basis of yeast prion strain variants. Nature *449*, 233–237.

True, H.L., and Lindquist, S.L. (2000). A yeast prion provides a mechanism for genetic variation and phenotypic diversity. Nature *407*, 477–483.

True, H.L., Berlin, I., and Lindquist, S.L. (2004). Epigenetic regulation of translation reveals hidden genetic variation to produce complex traits. Nature *431*, 184–187.

Uptain, S.M., Sawicki, G.J., Caughey, B., and Lindquist, S. (2001). Strains of [PSI(+)] are distinguished by their efficiencies of prion-mediated conformational conversion. EMBO J. *20*, 6236–6245.

Wang, Y., and Jardetzky, O. (2002). Probability-based protein secondary structure identification using combined NMR chemical-shift data. Protein Sci. *11*, 852–861.

Wasmer, C., Schütz, A., Loquet, A., Buhtz, C., Greenwald, J., Riek, R., Böckmann, A., and Meier, B.H. (2009). The molecular organization of the fungal prion HET-s in its amyloid form. J. Mol. Biol. *394*, 119–127.

Wiltzius, J.J.W., Landau, M., Nelson, R., Sawaya, M.R., Apostol, M.I., Goldschmidt, L., Soriaga, A.B., Cascio, D., Rajashankar, K., and Eisenberg, D. (2009). Molecular mechanisms for protein-encoded inheritance. Nat. Struct. Mol. Biol. *16*, 973–978.